2017

Human ribonuclease H1 resolves R-loops and thereby enables progression of the DNA replication fork

Shankar Parajuli
Washington University School of Medicine in St. Louis

Daniel C. Teasley
Washington University School of Medicine in St. Louis

Bhavna Murali
Washington University School of Medicine in St. Louis

Jessica Jackson
Saint Louis University

Alessandro Vindigni
Saint Louis University

See next page for additional authors

Human ribonuclease H1 resolves R-loops and thereby enables progression of the DNA replication fork

Received for publication, March 21, 2017, and in revised form, June 21, 2017 Published, Papers in Press, July 17, 2017, DOI 10.1074/jbc.M117.787473

Shankar Parajuli[‡], Daniel C. Teasley[‡], Bhavna Murali[‡], Jessica Jackson[§], Alessandro Vindigni[§¶1], and Sheila A. Stewart[‡¶‖2]**

*From the Departments of [‡]Cell Biology and Physiology and [‖]Medicine, [¶]Siteman Cancer Center, and **Integrating Communications within the Cancer Environment (ICCE) Institute, Washington University School of Medicine, St. Louis, Missouri 63110 and the [§]Edward A. Doisy Department of Biochemistry and Molecular Biology, Saint Louis University School of Medicine, St. Louis, Missouri 63104*

Edited by Patrick Sung

Faithful DNA replication is essential for genome stability. To ensure accurate replication, numerous complex and redundant replication and repair mechanisms function in tandem with the core replication proteins to ensure DNA replication continues even when replication challenges are present that could impede progression of the replication fork. A unique topological challenge to the replication machinery is posed by RNA–DNA hybrids, commonly referred to as R-loops. Although R-loops play important roles in gene expression and recombination at immunoglobulin sites, their persistence is thought to interfere with DNA replication by slowing or impeding replication fork progression. Therefore, it is of interest to identify DNA-associated enzymes that help resolve replication-impeding R-loops. Here, using DNA fiber analysis, we demonstrate that human ribonuclease H1 (RNH1) plays an important role in replication fork movement in the mammalian nucleus by resolving R-loops. We found that RNH1 depletion results in accumulation of RNA–DNA hybrids, slowing of replication forks, and increased DNA damage. Our data uncovered a role for RNH1 in global DNA replication in the mammalian nucleus. Because accumulation of RNA–DNA hybrids is linked to various human cancers and neurodegenerative disorders, our study raises the possibility that replication fork progression might be impeded, adding to increased genomic instability and contributing to disease.

High-fidelity DNA replication is paramount to the maintenance of genome stability. Therefore, cells have evolved various redundant mechanisms to resolve genotoxic challenges including the presence of topological structures. If not resolved, these structures can impede replication fork progression, leading to the stalling and eventual collapse of replication forks (1). One such structure is the RNA–DNA hybrid, commonly referred to as an R-loop. Mapping studies have revealed that RNA–DNA hybrid structures are present throughout the genome more frequently than previously appreciated (2, 3). One source of R-loops is transcription during which nascent RNA emanating from RNA polymerase II hybridizes with its template DNA (4). Although these topological structures play a vital role in a number of key processes including class switch recombination of immunoglobulin genes and transcription termination, their persistence or unscheduled formation and stabilization pose a significant challenge to genome integrity (5, 6). Because DNA replication and transcription occur simultaneously at many regions of the genome, hybrids can form in front of the replication machinery and affect its progression. Indeed, these R-loops can lead to increased DNA mutations, unwanted recombination, and gross chromosomal aberrations (7). Thus, it is not surprising that a number of proteins inhibit the formation of these structures or resolve them once they have formed (4). Topoisomerase I, mRNA export, and splicing factors, for example, play an active role in preventing R-loop formation (4, 8). Conversely, the helicases Senataxin (SETX)[3] and Aquarius (AQR) are tasked with resolving these structures to promote transcriptional termination and maintain genome stability, respectively (6, 9). In addition, DNA damage response factors such as breast cancer susceptibility factors (BRCA1 and BRCA2) are also implicated in preventing R-loop accumulation and the ensuing DNA damage (10, 11).

Ribonuclease H1 (RNH1) is a specialized enzyme that can specifically resolve long RNA–DNA hybrids. A closely related protein complex, ribonuclease H2 (RNH2), is adept at removing single misincorporated ribonucleotides from DNA and is critical for ongoing genomic stability (12). In yeast, RNH1 and RNH2 function redundantly to facilitate efficient double strand break repair during homologous recombination by assisting in the unwinding of DNA strands and replication protein A bind-

This work was supported by a Predoctoral Cancer Biology Pathway grant, Siteman Cancer Center/Barnes Jewish Hospital (to S. P.); National Institutes of Health Molecular Oncology Training Grant T32CA113275 (to B. M.); National Institutes of Health Grant R01GM108648 (to A. V.); United States Department of Defense Breast Cancer Research Program Breakthrough Award BC151728 (to A. V.); National Institutes of Health Grant CA130919 (to S. A. S.); and an American Cancer Society research scholar award (to S. A. S.). The authors declare that they have no conflicts of interest with the contents of this article. The content is solely the responsibility of the authors and does not necessarily represent the official views of the National Institutes of Health.

[1] To whom correspondence may be addressed. E-mail: avindign@slu.edu.
[2] To whom correspondence may be addressed. E-mail: sheila.stewart@wustl.edu.

[3] The abbreviations used are: SETX, Senataxin; AQR, Aquarius; RNAH, ribonuclease H; CO, chromosomal orientation; siCtrl, control siRNA; siRNH1, RNH1-directed siRNA; DIP, DNA–RNA immunoprecipitation; maRTA, microfluidic-assisted replication track analysis; CldU, 5-chloro-2′-deoxyuridine; IdU, 5-iodo-2′-deoxyuridine; BrdC, 5-bromo-2′-deoxycytidine; qRT, quantitative reverse transcription; γH2AX, histone H2AX phosphorylation at Ser-139; FAM, 6-fluorescein amidite.

ing (13). Ectopic expression of RNH1 in yeast is sufficient to minimize transcription-dependent hyper-recombination, pausing of the replication fork, and hydroxyurea sensitivity (14–16). In mammalian cells, RNH1 has an established role in mitochondrial DNA replication, and its deletion is embryonically lethal, demonstrating that RNH2 cannot compensate in this setting (17–20). RNH1 localizes to the mammalian nucleus (21), and ectopic RNH1 expression is routinely exploited in mammalian cells to resolve RNA–DNA hybrids. Recently, RNH1 was shown to prevent unwanted recombination events at the telomere by resolving telomeric RNA–DNA hybrids in cells that utilize the alternative lengthening mechanism of telomere maintenance (22). Another recent study identified a link between DNA damage and the accumulation of RNA–DNA hybrids at the telomere (23). However, whether RNH1 plays a role in nuclear DNA replication outside of telomeres remains to be explored.

Given the role of RNA–DNA hybrids in replication impairment and the ability of RNH1 to resolve such hybrids, we sought to determine whether RNH1 impacts genomic integrity in the mammalian nucleus and if so how. We depleted RNH1 from human cell lines and found that RNH1 depletion resulted in increased RNA–DNA hybrids, DNA damage response, and slowing of DNA replication forks. Importantly, these phenotypes were dependent upon RNH1 nuclease activity, suggesting that the hybrids were responsible for these phenotypes. Our studies uncover a novel role of RNH1 in the mammalian nucleus and extend its important function in nuclear DNA replication.

Results

RNH1 contributes to genome stability and preserves telomere integrity

Although RNH2 has well-ascribed functions in the mammalian nucleus, the role of RNH1 has remained more obscure. Because R-loops form throughout the genome and RNH1 can resolve R-loops that would pose barriers to the replication machinery, we hypothesized that RNH1 might play an important role in the nucleus and that its loss might perturb replication fork progression and thus elicit a DNA damage response (4). To test this hypothesis, we depleted RNH1 from normal, checkpoint-competent RPE1 cells and measured the levels of histone H2AX phosphorylation at Ser-139 (γH2AX), a canonical marker of the DNA damage response (24), in control *versus* RNH1-depleted cells. Following RNH1 depletion, we observed increased levels of γH2AX, demonstrating that RNH1 depletion induces a DNA damage response (Fig. 1, *A* and *B*). These data suggest that RNH1 plays an important role in preserving genome stability.

To further interrogate the function of RNH1, we first focused our attention to telomeres, chromosomal ends that contain RNA–DNA hybrids (25). Recent work demonstrates that in cells utilizing the alternative lengthening of telomere mechanism, which maintains telomere length independently of telomerase, RNH1 associates with telomeres and regulates the levels of telomeric RNA–DNA hybrids to prevent telomere loss (22). In these cells, depletion of RNH1 led to hybrid accumulation and abrupt telomere excision. A second study suggested that RNH1 plays an important role in resolving RNA–DNA hybrids at the telomere (23). Because the leading strand-replicated telomere is transcribed, RNA–DNA hybrids would be expected to form on the leading strand. Thus, we examined the integrity of the leading strand telomere by performing chromosomal orientation fluorescence *in situ* hybridization (CO-FISH), which allows one to interrogate the leading *versus* lagging strand-replicated telomere. Surprisingly, CO-FISH analysis revealed no differences in the leading *versus* lagging strand telomere in control *versus* shRNH1 cells (data not shown). However, in the RNH1-depleted cells, we observed a significant increase in telomere free ends in which both leading and lagging strand telomeres were lost, a phenotype suggestive of DNA replication defects (26) (Fig. 1, *C* and *D*). These data suggest that RNH1 assists the replication machinery by resolving RNA–DNA hybrids that could present a topological barrier to replication fork progression.

Nuclear RNA–DNA hybrid levels increase upon RNH1 depletion

To demonstrate that RNA–DNA hybrids were responsible for the DNA damage and telomere loss phenotype upon RNH1 loss, we next measured the hybrid levels in the nucleus. We treated 293T cells with control (siCtrl) or RNH1-directed (siRNH1) siRNAs and collected cells 48 h later. Transfection with siRNH1 led to a significant reduction in RNH1 mRNA levels (2.5-fold) (Fig. 2*A*) and protein levels (3.5-fold) (Fig. 2*B*) compared with levels present in siCtrl cells. To measure the amount of RNA–DNA hybrids in control *versus* RNH1-depleted cells, we next extracted nuclear DNA lysate and subjected it to DNA–RNA immunoprecipitation (DIP) using the well-characterized RNA–DNA hybrid antibody S9.6 (27). We conducted a genomic quantitative PCR on a well-characterized hybrid-forming 5′ pause site of β-actin gene as a readout of hybrids. As a control for specificity, we also pretreated lysates with recombinant RNaseH enzyme *in vitro* to degrade existing RNA–DNA hybrids in both control and depleted cells. As expected, pretreatment with an *in vitro* RNaseH enzyme led to a 1.8-fold reduction of RNA–DNA hybrids in control and a 3.5-fold in RNH1-depleted cells, confirming the specificity of the S9.6 antibody. Additionally, immunoprecipitation with an IgG control antibody failed to precipitate RNA–DNA hybrids, indicating that the signals we measured were *bona fide* RNA–DNA hybrids. Analysis of immunoprecipitations from RNH1-depleted cells revealed a significant 2-fold increase in the nuclear RNA–DNA hybrids compared with those in control cells (Fig. 2*C*). To further corroborate these findings, we also utilized the S9.6 antibody and carried out immunofluorescence on RPE1 cells. As expected, RNH1-depleted cells showed increased levels of RNA–DNA hybrids as represented by elevated S9.6 signal in the nucleus compared with that in the control cells (Fig. 2, *D* and *E*). Together, these data demonstrate that RNH1 depletion can lead to a significant increase in RNA–DNA hybrids and that this increase correlates with increased DNA damage and telomere loss.

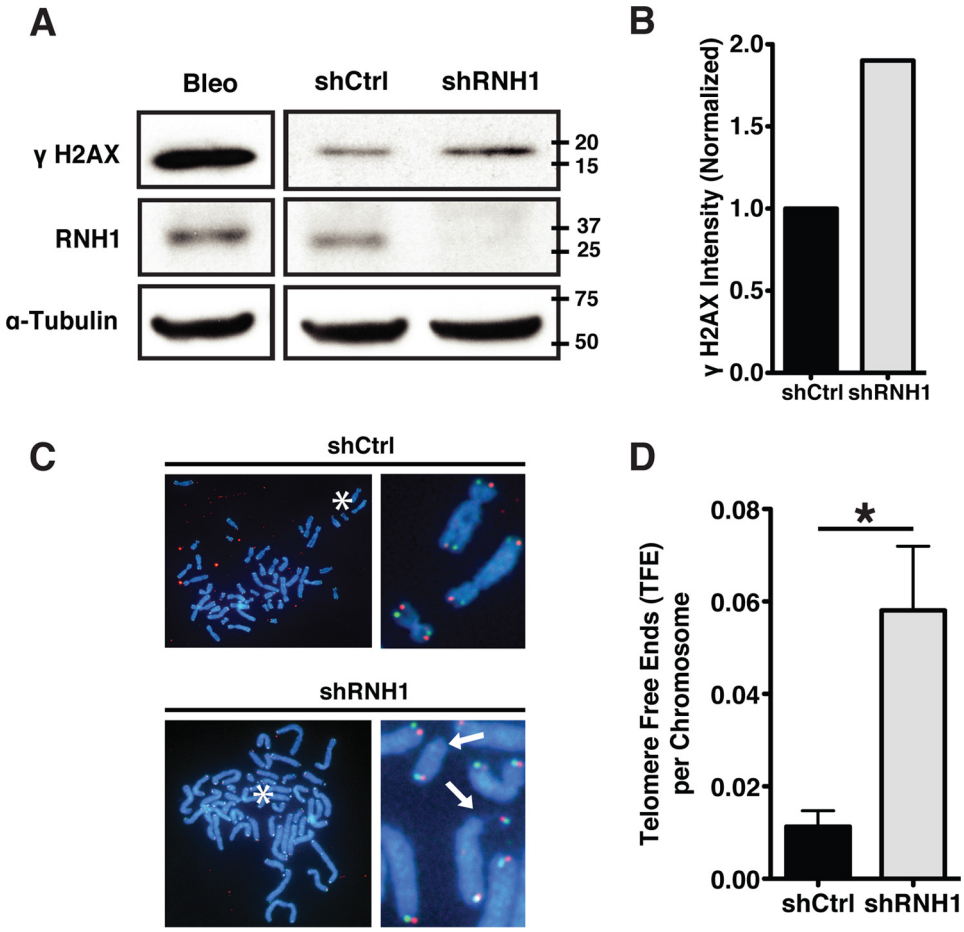

Figure 1. RNH1 contributes to genome stability and preserves telomere integrity. *A*, Western analysis of RNH1 expression and γH2AX in control (shCtrl) and RNH1-depleted RPE1 cells (shRNH1). Bleomycin-treated cells (*Bleo*) served as a positive control for γH2AX. α-Tubulin is shown as a loading control. Molecular mass in kilodaltons is marked to the *right* for reference. *B*, quantification of γH2AX intensity in shCtrl and shRNH1 cells from the Western blot in *A*. *C*, representative metaphase chromosomes processed with CO-FISH from shCtrl or shRNH1 RPE1 cells. Leading strand-replicated telomeres are *green*, and lagging strand-replicated telomeres are *red*. Regions marked by *white asterisks* are magnified; *white arrows* indicate telomere free ends (*TFE*) in magnified images. *D*, representative quantification of telomere loss in shCtrl and shRNH1 RPE1 cells. A minimum of 700 metaphase chromosomes were analyzed. *p* values were computed using a two-tailed Student's *t* test (*, $p < 0.05$). *Error bars* represent S.E.

RNH1 depletion results in replication fork slowing and increased termination and stalling

Given the increased RNA–DNA hybrids, DNA damage, and loss of both telomeric ends, indicative of a replication defect following RNH1 depletion, we hypothesized that RNA–DNA hybrids pose barriers to DNA replication forks. This hypothesis was supported by previous studies showing that the removal of RNA–DNA hybrids by ectopically expressed RNH1 can directly affect replication fork movement in yeast (28). To test this hypothesis, we used microfluidic-assisted replication track analysis (maRTA) to directly measure replication fork progression in RPE1 cells depleted of RNH1 (29, 30). RPE1 cells were transduced with siRNAs, and cells were collected for Western blot analysis 48 h later. As expected, RNH1 depletion resulted in significant DNA damage as evidenced by increased γH2AX (Fig. 3*A*). In parallel, we carried out maRTA by plating RNH1-depleted or control cells and labeling them with the nucleotide analogs CldU (red) and IdU (green) sequentially for 30 min each to allow us to follow replication fork movement (Fig. 3*B*). To restrict our analysis to progressing replication forks, we measured IdU tracks that were directly preceded by a CldU track (Fig. 3*B*). Measuring the lengths of these IdU tracks, we found that RNH1-depleted cells had an average IdU track length of 9.3 ± 0.3 μm, whereas that in the control cells was 14.5 ± 0.4 μm, indicating that the replication forks moved significantly slower in RNH1-depleted cells compared with control cells (Fig. 3*C*). Given the increase in RNA–DNA hybrids associated with RNH1 loss, these data suggest that RNH1 facilitates efficient DNA replication by clearing RNA–DNA hybrids that would otherwise impede replication fork progression during S phase.

To understand how the loss of RNH1 perturbed replication dynamics, we next asked whether other replication parameters including termination, stalling, and origin firing were affected upon RNH1 depletion. Premature termination and stalling events correspond to CldU (red)-only tracks (Fig. 3*B*). RNH1-depleted cells showed a significant 1.4-fold increase in termination and/or stalling events compared with control cells (Fig. 3*D*). Next, we analyzed the impact of RNH1 depletion on origin firing to address a possibility that slower fork progression triggers the S phase checkpoint and increases the frequency of origin firing as reported previously (31). To measure origin firing, the incidence of tracks with either green-only (IdU) color

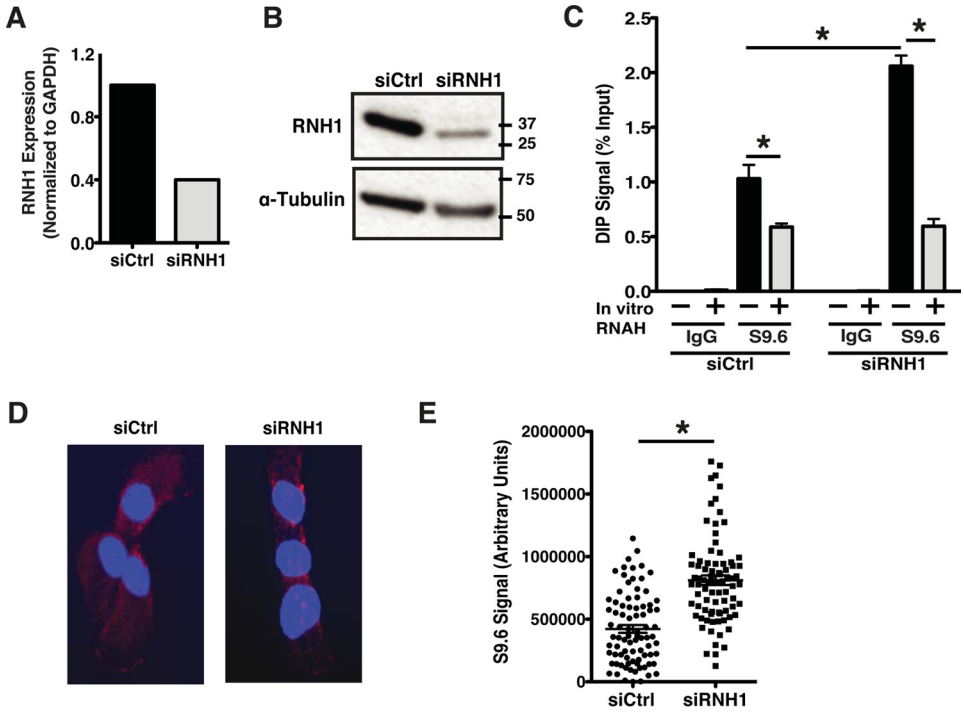

Figure 2. Nuclear RNA–DNA hybrid levels increase upon RNH1 depletion. *A*, qRT-PCR analysis of RNH1 mRNA in 293 T cells transfected with siCtrl or siRNH1. Expression levels were calculated using the $\Delta\Delta C_t$ method and normalized relative to GAPDH expression. *B*, Western analysis of RNH1 expression in siCtrl and RNH1-depleted 293T cells (siRNH1). α-Tubulin is shown as a loading control. Molecular mass in kilodaltons is marked to the *right* for reference. *C*, quantification of the DIP signal shown as a percentage of input in siCtrl and siRNH1 293T cells. Pretreatment of lysate with *in vitro* RNaseH (*RNAH*) enzyme serves as a control for RNA–DNA hybrids. IgG is a nonspecific antibody, whereas S9.6 is an RNA–DNA hybrid-specific antibody. Analysis of three technical repeats from a representative experiment is shown. *p* values were computed using a three-way analysis of variance with Sidak multiple comparison test (*, $p < 0.05$). *Error bars* represent S.E. *D*, representative images of S9.6 immunofluorescence on RPE1 control (siCtrl) and RNH1-depleted (siRNH1) cells. *Blue* staining marks the nuclei, and *red* is S9.6 signal (RNA–DNA hybrids). *E*, quantification of S9.6 signal (raw integrated density) (arbitrary units) for siCtrl and siRNH1 cells. Shown is one of three independent experiments where a minimum of 80 nuclei were analyzed per sample. *p* values were computed using a non-parametric Mann-Whitney test (*, $p < 0.05$). *Error bars* represent S.E.

or red flanked by green on both sides was analyzed (Fig. 3*B*). However, no significant differences in origin firing were observed between RNH1-depleted and control cells (Fig. 3*E*). Collectively, these results indicate that RNH1 plays an important role in assisting fork movement during DNA replication. We suggest that RNH1 does this by resolving RNA–DNA hybrids that pose barriers to a progressing replication fork. Furthermore, our data provide the first evidence that RNH1 plays a role in global DNA replication in the mammalian nucleus.

Nuclease activity of RNH1 is required for efficient replication fork movement

To further characterize the role of RNH1 in DNA replication, we tested whether the nuclease function of RNH1 was required for this activity. To do this, we created a series of RPE1 cell lines ectopically expressing either a GFP-tagged wild-type (WT) or a well-characterized GFP-tagged nuclease-dead (D145N) form of RNH1 (32, 33). To establish a direct role in the nucleus, these RNH1 constructs lacked the mitochondrial targeting sequence present in the endogenous gene, thereby restricting their expression to the nucleus. We confirmed the nuclear localization of ectopically expressed proteins by visualizing GFP expression only in the nucleus (Fig. 4*A*). These stable RPE1 cells were transfected with an siRNH1 directed toward the 3′-untranslated region (3′-UTR) that did not target the ectopically expressed protein. We observed that RNH1 depletion using a 3′-UTR siRNA was comparable with that of a previously used coding sequence targeting siRNA (Fig. 4*B*). We also observed robust expression of our ectopically tagged RNH1 proteins and significant depletion of endogenous RNH1 levels (Fig. 4*B*). Next, using maRTA, we again measured replication fork movement and found that ectopic expression of WT RNH1 restored fork movement to the levels observed in siCtrl cells (Fig. 4*C*). Indeed, although RNH1-depleted forks moved an IdU length of 8 μm, ectopic expression of WT RNH1 increased this to 12 μm, levels we observed in siCtrl cells. In contrast, ectopic expression of the catalytically dead D145N allele of RNH1 failed to rescue the replication fork movement defect (fork movement was 7.9 μm, nearly identical to that observed in RNH1-depleted cells). Together, these findings demonstrated that the nuclease activity of RNH1 is required for the unperturbed movement of replication forks in mammalian cells. Similarly, we also measured fork termination and stalling events upon ectopic expression of WT and D145N alleles in RNH1-depleted cells. As expected, both events were reversed by ectopic expression of WT RNH1 but not the nuclease-dead allele, thereby reiterating the importance of the nuclease function of RNH1 in the fidelity of replication fork progression (Fig. 4*D*). Neither WT nor the D145N allele of RNH1 affected the levels of origin firing in RNH1-depleted cells (Fig. 4*E*). These data suggest that the nuclease activity of RNH1 is required for resolution of RNA–DNA

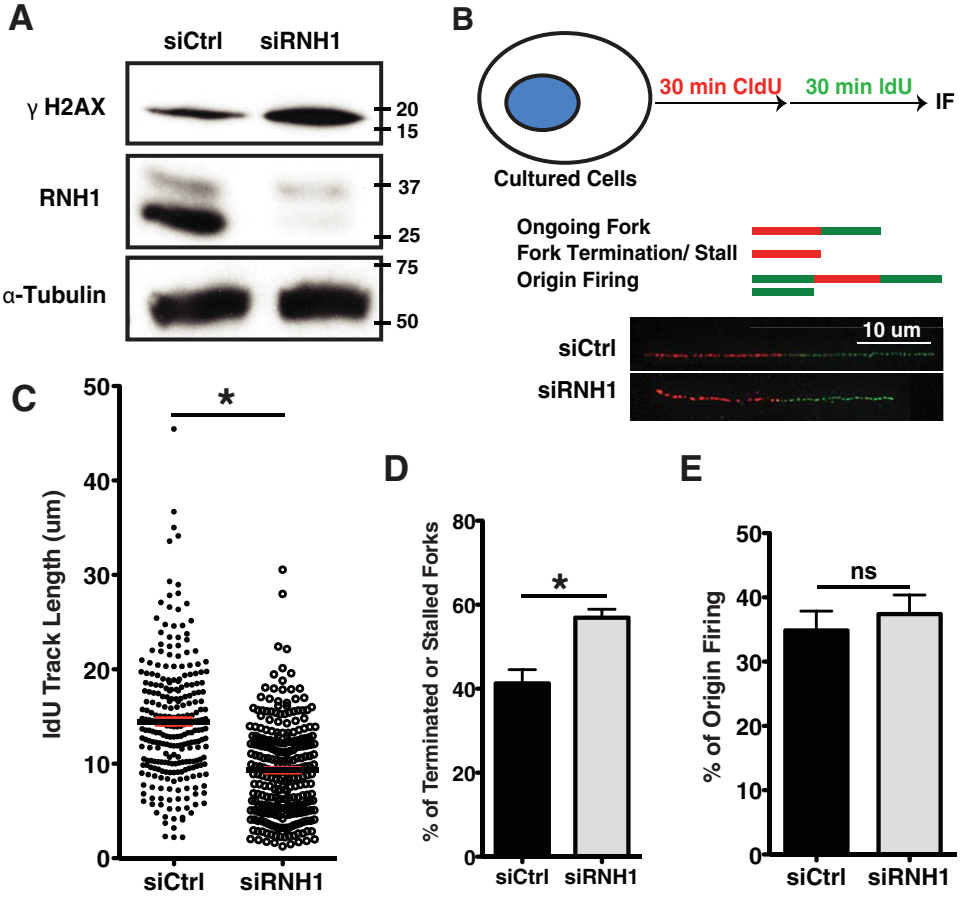

Figure 3. RNH1 depletion results in replication fork slowing and increased termination and stalling. *A*, Western analysis of RNH1 expression and γH2AX in RPE1 cells transfected with siCtrl and siRNH1. α-Tubulin is shown as a loading control. Molecular mass in kilodaltons is marked to the *right* for reference. *B*, schematics showing labeling of cells for maRTA. Transfected RPE1 cells were labeled with base analogs CldU and IdU for 30 min each and subjected to the maRTA protocol and DNA visualization in *red* (CldU) and *green* (IdU) by immunofluorescence (*IF*). Ongoing forks were marked by a red track (IdU) followed by green (CldU); terminated and/or stalled were red-only tracks; origin firings were both green-only and red flanking green on either side. Representative DNA tracks for siCtrl and siRNH1 samples are shown. *C*, a representative quantification of three independent biological experiments showing the IdU track length (μm) preceded by a CldU track. Analysis included a minimum of 260 two-color DNA tracks (moving fork) isolated from siCtrl and siRNH1 cells each. *p* values were computed using a two-tailed Student's *t* test (*, $p < 0.05$). *Error bars* represent S.E. *D*, quantification of percentage of termination and stalling events in DNA isolated from siCtrl and siRNH1 samples. Means from three independent experiments were analyzed, and each analysis included between 210 and 260 DNA tracks per sample. *p* values were computed using a two-tailed Student's *t* test (*, $p < 0.05$). *Error bars* represent S.E. *E*, quantification of the percentage of origin firings in DNA isolated from siCtrl and siRNH1 samples. The graph represents combined means from three independent experiments that included between 275 and 350 DNA tracks per sample. *p* values were computed using a two-tailed Student's *t* test (*ns*, $p > 0.05$). *Error bars* represent S.E.

hybrids and therefore efficient movement of replication forks during nuclear DNA replication.

Discussion

Our study establishes a role for RNH1 in genomic DNA replication. Indeed, we illustrate for the first time that RNH1 nuclease activity is required for efficient fork movement during nuclear DNA replication. Furthermore, we have established a correlation between the accumulation of RNA–DNA hybrids and replication defects observed upon RNH1 depletion. Taken together, we propose a model wherein RNH1 resolves RNA–DNA hybrids to assist the replication machinery in its uninterrupted movement during DNA replication.

The unscheduled formation and stabilization of RNA–DNA hybrids have been postulated to be detrimental to the replication machinery. The importance of resolving these structures is probably best underscored by the multitude of proteins that act on RNA–DNA structures. Indeed, helicases such as SETX, AQR, and DHX9 in mammalian cells and Sen1 and PIF1 in yeast have all been shown to resolve RNA–DNA hybrids (9, 34–36). Here, we add RNH1 to a growing list of proteins by showing that endogenous RNH1 is required to similarly remove RNA–DNA hybrids and that if these hybrids are not removed replication is significantly impacted. Furthermore, our work demonstrates that these other proteins are unable to compensate for loss of RNH1 in replication fork progression. However, how RNH1 is regulated in the nucleus and how its activity is coordinated with the replication machinery remain unclear. A recent study from Nguyen *et al.* (37) elegantly demonstrated that replication protein A can interact with RNH1 and stimulate its activity, raising the possibility that RNH1 is tightly regulated by the DNA replication and repair machinery.

Given that RNH1 loss elicits replication defects such as fork slowing, termination, and fork stalling, it will be critical to determine how this impacts checkpoint activation and cell cycle progression. Furthermore, understanding the fate of accumulated RNA–DNA hybrids upon RNH1 depletion is another interesting avenue worth pursuing. As previously

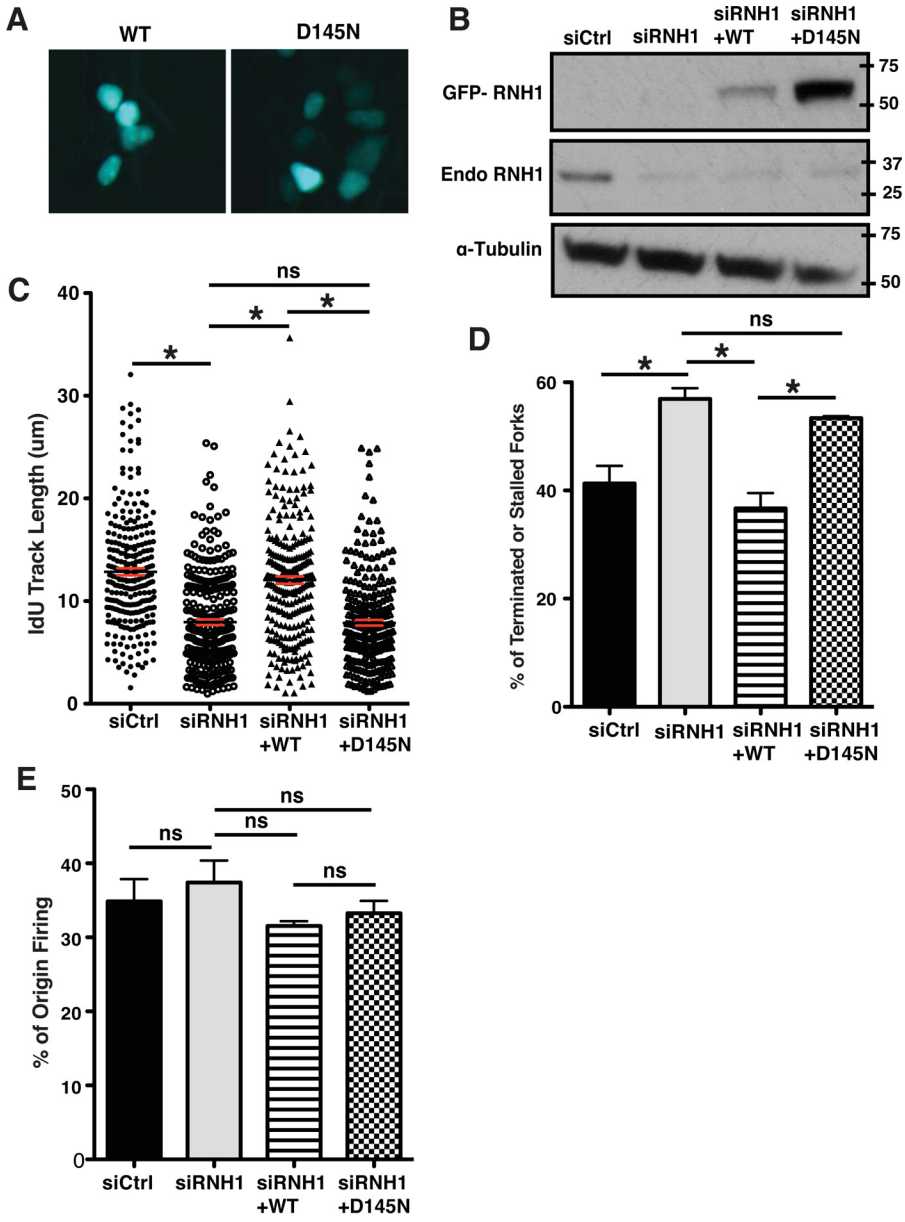

Figure 4. Nuclease activity of RNH1 is required for efficient replication fork movement. *A*, representative images verifying the nuclear localization (*green*) of ectopically expressed RNH1 in 293T cells transfected with a GFP-tagged WT RNH1 or nuclease-dead (D145N) allele. *B*, Western analysis of RNH1 expression (endogenous and ectopic) in RPE1 cells transfected with siCtrl or siRNH1 with or without ectopic expression of either GFP-tagged wild-type (siRNH1+ WT) or nuclease-dead (siRNH1+ D145N) RNH1. α-Tubulin is shown as a loading control. Molecular mass in kilodaltons is marked to the *right* for reference. *C*, a representative quantification of three independent biological experiments showing the IdU track length (μm) preceded by a CldU track. Analysis included 265–280 two-color DNA tracks (ongoing fork) isolated from each of the four samples. *p* values were computed using a one-way analysis of variance with Bonferroni multiple comparison test (*, $p < 0.05$; *ns*, $p > 0.05$). *Error bars* represent S.E. *D*, quantification of percentage of termination and stalling events in isolated DNA from all four samples. Means from three independent experiments were analyzed, and each analysis included between 240 and 350 DNA tracks per sample. *Error bars* represent S.E. *E*, quantification of the percentage of origin firings in DNA isolated from all four samples. The graph shown represents combined means from three independent experiments that included between 225 and 250 DNA tracks per sample. *Error bars* represent S.E.

noted, RNA–DNA hybrids arising from different sources can be processed via separate mechanisms (9). For example, those involved in class switch recombination are not processed via nucleotide excision repair, whereas those arising from loss of some RNA processing factors or camptothecin treatment are processed by nucleotide excision repair. It is also worth evaluating whether redundant nucleases and helicases including RNH2, SETX, and AQR could rescue the effects of RNH1 loss.

The study of R-loops and their resolution have sparked more attention in recent years due to the fact that R-loops are associated with a number of diseases including cancer and several neurodegenerative disorders (38). This underscores a need for understanding these structures and their origins, stabilization, and resolution along with their impact on cellular processes. By revealing the function of RNH1 in R-loop resolution in the nucleus, our study adds to the diversity of mechanisms targeting such structures. Furthermore,

our study identifies a previously unknown function of RNH1 in nuclear DNA replication. Together, our work broadens the understanding of RNA–DNA structures and places RNH1 as a novel mechanism to resolve those structures and assist in nuclear DNA replication.

Experimental procedures

Cell culture

Cells were cultured at 37 °C in 5% carbon dioxide and atmospheric oxygen as reported previously (39). 293T cells were obtained from Dr. Robert Weinberg (Massachusetts Institute of Technology) and cultured in high-glucose Dulbecco's modified Eagle's medium (DMEM) containing 10% heat-inactivated fetal bovine serum (FBS) and 1% penicillin/streptomycin (Sigma-Aldrich). RPE1 cells were obtained from ATCC and cultured in DMEM/Nutrient Mixture F-12 containing 7.5% heat-inactivated FBS and 1% penicillin/streptomycin.

siRNA transfection

siRNA transfection was performed using Invitrogen's Lipofectamine RNAiMAX reagent (Thermo Fisher Scientific) according to the manufacturer's protocol. siRNAs used were siCtrl (catalog number 4390843) and siRNH1 (catalog number 4390824, ID s48356) from Life Technologies or siRNA directed to the 3′-UTR of RNH1 (hs.Ri.RNASEH1.13.1) from Integrated DNA Technologies.

Virus production, infections, and stable cell lines

Lentiviral production and transductions were carried out as reported previously (40). Briefly, 293T cells were transduced with pLKO.1-puro plasmid carrying an shRNA using TransIT-LT1 reagent (Mirus Bio, Madison, WI) and a mixture containing 8:1 ratio of pHR-CMV-8.2 R packaging plasmid and pCMV-VSV-G. Supernatant containing virus was collected 48 h post-transfection and filtered through a 0.45-μm PVDF membrane. RPE1 cells were infected for 4 h each on 2 consecutive days in the presence of 8 μg/ml protamine sulfate (Sigma). Following infection, transduced cells were selected with 15 μg/ml puromycin sulfate. Stable RPE1 cell lines were prepared by using either a GFP-tagged D145N RNH1 construct (a generous gift from Dr. Marteijn) (32) or its wild-type version (modified from D145N construct using site-directed mutagenesis; Agilent Technologies).

Western blot analysis

Western blot analysis was carried out as described previously with modifications (41). Briefly, cells were washed with PBS and lysed in radioimmunoprecipitation assay buffer (150 mM NaCl, 50 mM Tris-HCl, pH 8.0, 1.0% Nonidet P-40, 0.5% sodium deoxycholate, and 0.1% SDS) supplemented with 1 mM sodium orthovanadate, 1 mM sodium fluoride, 1 mM microcystin LR, 2 mM phenylmethylsulfonyl fluoride, protease inhibitor mixture (Sigma), and phosphatase inhibitor mixture set I (EMD Millipore, Billerica, MA). Following sonication and centrifugation, supernatant lysate was quantified using a protein assay (Bio-Rad). Lysates were subjected to SDS-PAGE and transferred to PVDF membranes for blotting. The following antibodies were used: mouse monoclonal anti-RNase H1 (H00246243-M01, Novus Biologicals, Littleton, CO), rat monoclonal anti-tubulin (NB600-506, Novus Biologicals), and mouse monoclonal anti-phospho(Ser-139) H2AX (05-636, Millipore).

Metaphase chromosome preparation

Metaphase chromosomes were prepared as described previously (42). Briefly, cultured RPE1 cells were treated with 0.5 μg/ml Colcemid (Sigma) for 6 h. Arrested metaphase cells were collected by mitotic shake-off, treated with 75 mM potassium chloride, and fixed in 3:1 solution of methanol and acetic acid. Chromosomes were spread by dropping onto glass slides. For analysis via CO-FISH, 0.3 μg/ml BrdU (Sigma) and 0.1 μg/ml BrdC (MP Biomedicals, Santa Ana, CA) were added to the cultured medium 18 h prior to collection of the cells.

CO-FISH

CO-FISH was performed as described previously with modifications (43). Briefly, spread metaphase chromosomes were aged at 65 °C for 18 h. Aged chromosomes were rehydrated in PBS, treated with 100 μg/ml RNase at 37 °C for 10 min, and refixed in 4% paraformaldehyde at room temperature for 10 min. Fixed chromosomes were UV-sensitized in 0.5 μg/ml Hoechst 33258 (Sigma) in 2× SSC at room temperature for 15 min and exposed to 365 nm UV light for 1 h using a UV cross-linker (Vilber-Lourmat, Marne-la-Vallée, France). Exposed chromosomes were digested with 3 units/μl exonuclease III (Promega, Madison, WI) at room temperature for 15 min, denatured in 70% formamide in 2× SSC, and dehydrated in cold ethanol before hybridization. Chromosomes were hybridized first using a 0.03 μg/ml concentration of a leading strand telomere PNA probe (FAM-$(TTAGGG)_3$) followed by a 0.03 μg/ml concentration of a lagging strand PNA probe (Cy3-$(CCCTAA)_3$) (both probes from PNA Bio, Thousand Oaks, CA). Hybridized chromosomes were mounted using ProLong Gold (Life Technologies) with 125 ng/ml DAPI.

maRTA

maRTA was conducted as described previously (29, 44). Briefly, asynchronous RPE1 cells were labeled for 30 min each with 50 μM CldU and 50 μM IdU with two PBS washes in between. Labeled cells were collected and embedded in agarose plugs for lysis and DNA extraction. DNA was subsequently stretched, denatured, and subjected to immunostaining. Antibodies used were rat anti-CldU/BrdU (Abcam, ab6326), mouse anti-IdU/BrdU (BD Biosciences, 347580), goat anti-rat Alexa Fluor 594 (Invitrogen, A11007), and goat anti-mouse Alexa Fluor 488 (Invitrogen, A11001).

Fluorescence imaging

Metaphase chromosomes from CO-FISH and labeled DNA tracks from maRTA were imaged on a Nikon 90i epifluorescence microscope using a 100× 1.40 numerical aperture Plan Apo VC objective (Nikon Instruments, Melville, NY) with Cargille Type LDF immersion oil (Cargille Sacher Laboratories, Cedar Grove, NJ). Images were captured using a CoolSnap HQ2 charge-coupled device camera (Photometrics, Tucson, AZ) and deconvoluted with a blind algorithm using NISElements AR

(Nikon Instruments) prior to quantification. RPE1 cells stably expressing GFP-tagged WT and D145N RNH1 were visualized and captured without any staining.

DIP

DIP was performed as described previously with modifications (6). Briefly, 293T cells were pelleted and resuspended in DIP lysis buffer (0.5% Nonidet P-40, 85 mM potassium chloride, and 5 mM PIPES). Following centrifugation, pelleted nuclei were lysed in DIP nuclear lysis buffer (1% sodium dodecyl sulfate, 25 mM Tris-HCl, pH 8, and 5 mM EDTA), sheared, and digested with two sequential rounds of 100 μg of proteinase K for 1.5 h each at 55 °C. DNA was phenol/chloroform-extracted and ethanol-precipitated (45) at which point one-half was subjected to an overnight digestion with recombinant ribonuclease H (Roche Applied Science). Samples were then diluted in DIP dilution buffer (1.1% Triton X-100, 0.01% sodium dodecyl sulfate, 1.2 mM EDTA, 16.7 mM Tris-HCl, pH 8, and 166.5 mM sodium chloride) and sonicated to generate ~200-bp-long DNA fragments. Resulting DNA was quantified using the PicoGreen assay following the manufacturer's protocol (Life Technologies). 10 μg of DNA was immunoprecipitated overnight with 10 μg of S9.6 antibody or mouse IgG. Antibody–DNA complexes were captured by using Protein A magnetic beads (Life Technologies) after equilibration in DIP dilution buffer. After extensive washing, antibody–DNA complexes were eluted from the beads and treated with proteinase K followed by recovery using PCR clean-up columns (Qiagen, Venlo, Netherlands).

S9.6 immunofluorescence

S9.6 immunofluorescence was performed as described previously (9). Briefly, RPE1 cells transfected with siCtrl or siRNH1 were fixed with ice-cold methanol for 5 min at −20 °C. Fixed cells were blocked in 2% BSA and PBS for an hour at room temperature followed by incubation with the S9.6 primary antibody (1:200 dilution; 1 μg/ml) and goat anti-mouse Alexa Fluor 594-conjugated secondary antibody (1:1000) for 1 h each at room temperature. Finally, cells were washed in 0.5 μg/ml Hoechst 33258 in PBS to label the nuclei and mounted using ProLong Gold. Images were taken at 40× using a Nikon 90i epifluorescence microscope as described above. Only the nuclear staining of S9.6 signal was considered and analyzed using ImageJ 1.50i.

Genomic quantitative PCR

Genomic quantitative PCR was performed using Power SYBR Green Master Mix (Life Technologies) following the manufacturer's protocol. The 5′ region of the β-actin pause element (5′ pause site), known to form RNA–DNA hybrids, was amplified to assess hybrid formation. Reaction conditions were as described in the manufacturer's instructions with 58.7 °C as the annealing temperature. Primers used were: 5′-TTACCC AGA GTG CAG GTG TG-3′ (forward) and 5′-CCC CAA TAA GCA GGA ACA GA-3′ (reverse).

Quantitative reverse transcription-PCR (qRT-PCR)

qRT-PCR was performed as described previously (39). Target genes used were RNH1 (Hs00268000_m1, Life Technologies) and GAPDH (Hs.PT.39a.22214836, Integrated DNA Technologies).

Author contributions—Experiments were designed by S. A. S., A. V., S. P., and D. C. T. Experiments were performed by S. P., D. C. T., and J. J. Data were analyzed by S. A. S., A. V., B. M., and S. P. The manuscript was written by S. A. S., A. V., and S. P.

Acknowledgments—We thank Kevin C. Flanagan for helpful comments and Sandra Crocker and Shashikant Kulkarni for examination of chromosomes. We also thank Zhongsheng You for antibodies.

References

1. O'Driscoll, M. (2017) The pathological consequences of impaired genome integrity in humans; disorders of the DNA replication machinery. *J. Pathol.* **241,** 192–207
2. Ginno, P. A., Lim, Y. W., Lott, P. L., Korf, I., and Chédin, F. (2013) GC skew at the 5′ and 3′ ends of human genes links R-loop formation to epigenetic regulation and transcription termination. *Genome Res.* **23,** 1590–1600
3. Wongsurawat, T., Jenjaroenpun, P., Kwoh, C. K., and Kuznetsov, V. (2012) Quantitative model of R-loop forming structures reveals a novel level of RNA-DNA interactome complexity. *Nucleic Acids Res.* **40,** e16
4. Santos-Pereira, J. M., and Aguilera, A. (2015) R loops: new modulators of genome dynamics and function. *Nat. Rev. Genet.* **16,** 583–597
5. Yu, K., Chedin, F., Hsieh, C.-L., Wilson, T. E., and Lieber, M. R. (2003) R-loops at immunoglobulin class switch regions in the chromosomes of stimulated B cells. *Nat. Immunol.* **4,** 442–451
6. Skourti-Stathaki, K., Proudfoot, N. J., and Gromak, N. (2011) Human senataxin resolves RNA/DNA hybrids formed at transcriptional pause sites to promote Xrn2-dependent termination. *Mol. Cell* **42,** 794–805
7. Aguilera, A., and García-Muse, T. (2012) R loops: from transcription byproducts to threats to genome stability. *Mol. Cell* **46,** 115–124
8. Li, M., Pokharel, S., Wang, J.-T., Xu, X., and Liu, Y. (2015) RECQ5-dependent SUMOylation of DNA topoisomerase I prevents transcription-associated genome instability. *Nat. Commun.* **6,** 6720
9. Sollier, J., Stork, C. T., García-Rubio, M. L., Paulsen, R. D., Aguilera, A., and Cimprich, K. A. (2014) Transcription-coupled nucleotide excision repair factors promote R-loop-induced genome instability. *Mol. Cell* **56,** 777–785
10. Bhatia, V., Barroso, S. I., García-Rubio, M. L., Tumini, E., Herrera-Moyano, E., and Aguilera, A. (2014) BRCA2 prevents R-loop accumulation and associates with TREX-2 mRNA export factor PCID2. *Nature* **511,** 362–365
11. Hatchi, E., Skourti-Stathaki, K., Ventz, S., Pinello, L., Yen, A., Kamieniarz-Gdula, K., Dimitrov, S., Pathania, S., McKinney, K. M., Eaton, M. L., Kellis, M., Hill, S. J., Parmigiani, G., Proudfoot, N. J., and Livingston, D. M. (2015) BRCA1 recruitment to transcriptional pause sites is required for R-loop-driven DNA damage repair. *Mol. Cell* **57,** 636–647
12. Reijns, M. A., Rabe, B., Rigby, R. E., Mill, P., Astell, K. R., Lettice, L. A., Boyle, S., Leitch, A., Keighren, M., Kilanowski, F., Devenney, P. S., Sexton, D., Grimes, G., Holt, I. J., Hill, R. E., *et al.* (2012) Enzymatic removal of ribonucleotides from DNA is essential for mammalian genome integrity and development. *Cell* **149,** 1008–1022
13. Ohle, C., Tesorero, R., Schermann, G., Dobrev, N., Sinning, I., and Fischer, T. (2016) Transient RNA-DNA hybrids are required for efficient double-strand break repair. *Cell* **167,** 1001.e7–1013.e7
14. Huertas, P., and Aguilera, A. (2003) Cotranscriptionally formed DNA: RNA hybrids mediate transcription elongation impairment and transcription-associated recombination. *Mol. Cell* **12,** 711–721
15. Wellinger, R. E., Prado, F., and Aguilera, A. (2006) Replication fork progression is impaired by transcription in hyperrecombinant yeast cells lacking a functional THO complex. *Mol. Cell. Biol.* **26,** 3327–3334
16. Gómez-González, B., Felipe-Abrio, I., and Aguilera, A. (2009) The S-phase checkpoint is required to respond to R-loops accumulated in THO mutants. *Mol. Cell. Biol.* **29,** 5203–5213

17. Ruhanen, H., Ushakov, K., and Yasukawa, T. (2011) Involvement of DNA ligase III and ribonuclease H1 in mitochondrial DNA replication in cultured human cells. *Biochim. Biophys. Acta* **1813,** 2000–2007
18. Lima, W. F., Murray, H. M., Damle, S. S., Hart, C. E., Hung, G., De Hoyos, C. L., Liang, X. H., and Crooke, S. T. (2016) Viable RNaseH1 knockout mice show RNaseH1 is essential for R loop processing, mitochondrial and liver function. *Nucleic Acids Res.* **44,** 5299–5312
19. Cerritelli, S. M., Frolova, E. G., Feng, C., Grinberg, A., Love, P. E., and Crouch, R. J. (2003) Failure to produce mitochondrial DNA results in embryonic lethality in Rnaseh1 null mice. *Mol. Cell* **11,** 807–815
20. Cerritelli, S. M., and Crouch, R. J. (2009) Ribonuclease H: the enzymes in eukaryotes. *FEBS J.* **276,** 1494–1505
21. Suzuki, Y., Holmes, J. B., Cerritelli, S. M., Sakhuja, K., Minczuk, M., Holt, I. J., and Crouch, R. J. (2010) An upstream open reading frame and the context of the two AUG codons affect the abundance of mitochondrial and nuclear RNase H1. *Mol. Cell. Biol.* **30,** 5123–5134
22. Arora, R., Lee, Y., Wischnewski, H., Brun, C. M., Schwarz, T., and Azzalin, C. M. (2014) RNaseH1 regulates TERRA-telomeric DNA hybrids and telomere maintenance in ALT tumour cells. *Nat. Commun.* **5,** 5220
23. Sagie, S., Toubiana, S., Hartono, S. R., Katzir, H., Tzur-Gilat, A., Havazelet, S., Francastel, C., Velasco, G., Chédin, F., and Selig, S. (2017) Telomeres in ICF syndrome cells are vulnerable to DNA damage due to elevated DNA: RNA hybrids. *Nat. Commun.* **8,** 14015
24. Siddiqui, M. S., François, M., Fenech, M. F., and Leifert, W. R. (2015) Persistent γH2AX: a promising molecular marker of DNA damage and aging. *Mutat. Res. Rev. Mutat. Res.* **766,** 1–19
25. Azzalin, C. M., Reichenbach, P., Khoriauli, L., Giulotto, E., and Lingner, J. (2007) Telomeric repeat containing RNA and RNA surveillance factors at mammalian chromosome ends. *Science* **318,** 798–801
26. Takikawa, M., Tarumoto, Y., and Ishikawa, F. (2017) Fission yeast Stn1 is crucial for semi-conservative replication at telomeres and subtelomeres. *Nucleic Acids Res.* **45,** 1255–1269
27. Boguslawski, S. J., Smith, D. E., Michalak, M. A., Mickelson, K. E., Yehle, C. O., Patterson, W. L., and Carrico, R. J. (1986) Characterization of monoclonal antibody to DNA.RNA and its application to immunodetection of hybrids. *J. Immunol. Methods* **89,** 123–130
28. Jones, R. M., Mortusewicz, O., Afzal, I., Lorvellec, M., García, P., Helleday, T., and Petermann, E. (2013) Increased replication initiation and conflicts with transcription underlie Cyclin E-induced replication stress. *Oncogene* **32,** 3744–3753
29. Berti, M., Ray Chaudhuri, A., Thangavel, S., Gomathinayagam, S., Kenig, S., Vujanovic, M., Odreman, F., Glatter, T., Graziano, S., Mendoza-Maldonado, R., Marino, F., Lucic, B., Biasin, V., Gstaiger, M., Aebersold, R., *et al.* (2013) Human RECQ1 promotes restart of replication forks reversed by DNA topoisomerase I inhibition. *Nat. Struct. Mol. Biol.* **20,** 347–354
30. Sidorova, J. M., Li, N., Schwartz, D. C., Folch, A., and Monnat, R. J. (2009) Microfluidic-assisted analysis of replicating DNA molecules. *Nat. Protoc.* **4,** 849–861
31. Zhong, Y., Nellimoottil, T., Peace, J. M., Knott, S. R., Villwock, S. K., Yee, J. M., Jancuska, J. M., Rege, S., Tecklenburg, M., Sclafani, R. A., Tavaré, S., and Aparicio, O. M. (2013) The level of origin firing inversely affects the rate of replication fork progression. *J. Cell. Biol.* **201,** 373–383
32. Tresini, M., Warmerdam, D. O., Kolovos, P., Snijder, L., Vrouwe, M. G., Demmers, J. A., van IJcken, W. F., Grosveld, F. G., Medema, R. H., Hoeijmakers, J. H., Mullenders, L. H., Vermeulen, W., and Marteijn, J. A. (2015) The core spliceosome as target and effector of non-canonical ATM signalling. *Nature* **523,** 53–58
33. Wu, H., Lima, W. F., and Crooke, S. T. (2001) Investigating the structure of human RNase H1 by site-directed mutagenesis. *J. Biol. Chem.* **276,** 23547–23553
34. Chakraborty, P., and Grosse, F. (2011) Human DHX9 helicase preferentially unwinds RNA-containing displacement loops (R-loops) and G-quadruplexes. *DNA Repair* **10,** 654–665
35. Mischo, H. E., Gómez-González, B., Grzechnik, P., Rondón, A. G., Wei, W., Steinmetz, L., Aguilera, A., and Proudfoot, N. J. (2011) Yeast Sen1 helicase protects the genome from transcription-associated instability. *Mol. Cell* **41,** 21–32
36. Boulé, J. B., and Zakian, V. A. (2007) The yeast Pif1p DNA helicase preferentially unwinds RNA-DNA substrates. *Nucleic Acids Res.* **35,** 5809–5818
37. Nguyen, H. D., Yadav, T, Giri, S., Saez, B., Graubert, T. A., and Zou, L. (2017) Functions of replication protein A as a sensor of R loops and a regulator of RNaseH1. *Mol. Cell* **65,** 832.e4–847.e4
38. Richard, P., and Manley, J. L. (2016) R loops and links to human disease. *J. Mol. Biol.* 10.1016/j.jmb.2016.08.031
39. Teasley, D. C., Parajuli, S., Nguyen, M., Moore, H. R., Alspach, E., Lock, Y. J., Honaker, Y., Saharia, A., Piwnica-Worms, H., and Stewart, S. A. (2015) Flap endonuclease 1 limits telomere fragility on the leading strand. *J. Biol. Chem.* **290,** 15133–15145
40. Stewart, S. A., Dykxhoorn, D. M., Palliser, D., Mizuno, H., Yu, E. Y., An, D. S., Sabatini, D. M., Chen, I. S., Hahn, W. C., Sharp, P. A., Weinberg, R. A., and Novina, C. D. (2003) Lentivirus-delivered stable gene silencing by RNAi in primary cells lentivirus-delivered stable gene silencing by RNAi in primary cells. *RNA* **9,** 493–501
41. Honaker, Y., and Piwnica-Worms, H. (2010) Casein kinase 1 functions as both penultimate and ultimate kinase in regulating Cdc25A destruction. *Oncogene* **29,** 3324–3334
42. Lansdorp, P. M., Verwoerd, N. P., van de Rijke, F. M., Dragowska, V., Little, M. T., Dirks, R. W., Raap, A. K., and Tanke, H. J. (1996) Heterogeneity in telomere length of human chromosomes. *Hum. Mol. Genet.* **5,** 685–691
43. Bailey, S. M., Cornforth, M. N., Kurimasa, A., Chen, D. J., and Goodwin, E. H. (2001) Strand-specific postreplicative processing of mammalian telomeres. *Science* **293,** 2462–2465
44. Schlacher, K., Christ, N., Siaud, N., Egashira, A., Wu, H., and Jasin, M. (2011) Double-strand break repair-independent role for BRCA2 in blocking stalled replication fork degradation by MRE11. *Cell* **145,** 529–542
45. Sambrook, J., Fritsche, E. F., and Maniatis, T. (1989) *Molecular Cloning: A Laboratory Manual*, 2nd Ed., Chapter 7, Cold Spring Harbor Laboratory Press, Plainview, NY

Human ribonuclease H1 resolves R-loops and thereby enables progression of the DNA replication fork

Shankar Parajuli, Daniel C. Teasley, Bhavna Murali, Jessica Jackson, Alessandro Vindigni and Sheila A. Stewart

J. Biol. Chem. 2017, 292:15216-15224.
doi: 10.1074/jbc.M117.787473 originally published online July 17, 2017